Facing the future of cosmetics: the first mitochondria-targeted delivery system for antiaging treatments

Grimaldi, Natascia[1]; Vasconcelos, Aimee[1]; Bellacanzone, Christian[1]; Nestor, Jeremie[1]; Ginestá, Albert[1] **Grimaldi, Natascia**[1*];

[1] Infinitec Activos (Evonik Nutrition & Care), Barcelona, Spain

＊ Grimaldi Natascia, C/Baldiri Reixac 4-8, CL03C61-2-3-4 Edifici Cluster, Parc Cientific de Barcelona 08028 (Barcelona, Spain), +34 934020160, Natascia.Grimaldi@evonik.com

Abstract (Maximum of 250 words)

Background: Mitochondria are responsible to produce the 90% of the cell energy, in the form of ATP. While producing energy, mitochondria generate ROS as by-products, which are neutralized by endogenous antioxidants (i.e. CoQ_{10}). Unfortunately, with the age the antioxidants production decrease, and ROS are accumulated, causing cells damage and death. Supplemented CoQ_{10} is a perfect ally to counteract skin aging, since it has both energizing and antioxidant effects. However, CoQ_{10} full potential can be only exploited when this is effectively delivered to mitochondria. Thus, at Infinitec (Evonik), we have recently developed a cutting-edge delivery system, named Trojan®, to encapsulate CoQ_{10} and effectively deliver it to mitochondria within fibroblast.

Methods: Physicochemical characterization (DLS, TEM, XPS) has been performed to prove the formation of PLGA particles and the surface functionalization with two peptides to target mitochondria within fibroblast. In vitro assay together with confocal and fluorescence microscopy has been used to test the efficacy of Trojan®Q10. Finally, the clinical efficacy of Trojan®Q10 was proved assessing the skin firmness and elasticity in the crow's feet area through Cutometer®.

Results: Trojan®Q10 can reach mitochondria within fibroblast, as showed by confocal microscopy, while the antioxidant activity has been demonstrated by restoring the mitochondria membrane potential, reducing the ROS level and increase the collagen IV and VII production. Finally, clinical study showed the efficacy of topical treatment with Trojan®Q10 to increase skin firmness and elasticity.

Conclusion: Trojan®Q10 effectively transport CoQ_{10} to fibroblast mitochondria where can behave as antioxidant leading to a final anti-aging activity.

Introduction.

Mitochondria play a pivotal role in the homeostasis of vital physiological functions.[1-2] Such subcellular organelles act as the cell's powerhouse, supplying 90% of the cellular energy in the form of ATP through the electron transport chain (ETC). The mitochondrial ETC creates an electrochemical gradient across the membrane through a series of redox reactions, which drives ATP synthesis and generates the mitochondrial membrane potential (MMP), a crucial parameter for evaluating mitochondrial function.

Mitochondria are also the main intracellular source of endogenous reactive oxygen species (ROS) generation because of electron transfer. In physiological condition, the cell defence mechanism regulates ROS production. Whereas excessive production occurs in mitochondria with altered functions, generating an imbalance that induces oxidative stress.[3-4] Growing evidence connects the mitochondria generated ROS and their accumulation to the pathogenesis of ageing [5-7] being the basis of the "The free radical theory of aging".

Several studies have revealed a strong positive correlation between MMP and reactive oxygen species production,[8] demonstrating that ROS production dramatically increases at high membrane potential (above 140mV), while a significant reduction occurs even at slight decrease (10mV).[9-11] In this regard, the focus on restoring the normal MMP, has assumed increasing importance for its impact on the whole-cell metabolism and function related to the process of aging. Therefore, the mitochondria have become an attractive target for delivering treatment, including antioxidants such as ubiquinone.

Coenzyme Q or ubiquinone, with Coenzyme Q_{10} (CoQ_{10}) being the predominant form of ubiquinone in human, is a lipophilic molecule present in all tissues and cells located mainly in the inner mitochondrial membrane, where it acts as a diffusible electron carrier in the mitochondrial respiratory chain. Coenzyme Q also functions as an antioxidant, scavenges oxygen reactive species, and is involved in multiple aspects of cellular metabolism.[12] In the frame of aging, CoQ_{10} is a powerful biomolecule, exhibiting both energizing and protecting

(anti-oxidative) effects on skin being an effective tool to fight aging. Unfortunately, endogenous CoQ_{10} levels into the skin decline with age, thus exposing the cells to a reduced mitochondrial protection. Several studies have revealed the beneficial effects of CoQ_{10} administration. However, its high molecular weight and low aqueous solubility limit is cellular uptake hampering its use as a therapeutic agent. Therefore, the delivery of CoQ_{10} directly to the mitochondria through the development of effective delivery systems is a prerogative to achieve the desired effect, improving its efficiency.

Among the different delivery systems, PLGA (Poly(D,L lactide-co-glycolide)) particles have been intensively explored by academia and industry, owing to the beneficial properties of this biopolymers. Beyond these properties, the polymer functionalization guarantees by the carboxylic group is of great relevance, since it provides targeting features to the delivery system, as shown by the growing trend towards the functionalization of the PLGA particles targeting specific cells.[13] One of the most explored solutions relies on the conjugation of cell-penetrating peptide (CPP) onto the surface of the particles.[14-18] CPPs are short peptides that can cross the cellular membrane and transport bioactive cargo into cells thus enhancing the efficacy of the delivered drug at a lower dose in a nontoxic way.[19-24]

A further progress in the PLGA particles selectivity involves targeting specific cells organelles such as mitochondria in order to achieve a more precise accumulation of NPs, making the treatment more effective.[25-26] Such objective has been recently achieved through the development of mitochondria-penetrating peptides (MPPs). These peptides are usually composed of alternating aromatic or hydrophobic residues and basic amino acids, and they accumulate preferentially in mitochondria.[27]

At Infinitec (Evonik), we have recently developed a cutting-edge delivery system composed of PLGA sub-micrometric particles functionalized with two different peptides for dual-mode cellular targeting and loaded with CoQ_{10}, namely Trojan®Q10. The new delivery system stabilizes the CoQ_{10} in the formula, enhancing its skin penetration. Furthermore, Trojan®Q10 is designed to reach mitochondria in specific cell-line, the fibroblasts, where releasing the antioxidant agent, CoQ_{10}, to reduce oxidative stress involved in the aging pathogenesis. The first peptide is a cell-penetrating peptide (Pentapeptide-4), that can be recognized by fibroblast growth factor receptors and promote Trojan®Q10 internalization in fibroblasts. The

second peptide (D-Arginyl Tyrosinyl Ornithinyl Phenylalanine) is a mitochondrion penetrating peptides, which has been designed to promote the passage of Trojan®Q10 across the mitochondrial membranes. Once the PLGA particles are localized at the mitochondrial level, they start to degrade and release Coenzyme Q_{10}. The delivered CoQ_{10} can participate in mitochondrial respiration, increasing mitochondria activity and ATP production and effectively neutralizing mROS acting on the mitochondrial membrane potential.

Materials and Methods.

Synthesis of activated PLGA-NHS polymer. Poly(D,L lactide-co-glycolide) (PLGA) was added to 5mL of chloroform in a tightly sealed vial under magnetic stirring. Then, 45mg of ethyl-3-(3-dimethyl aminopropyl) carbodiimideydrochloride (EDC) and 27mg of N-hydroxysuccinimide (NHS) were added, and the mixture was stirred overnight. The preactivated PLGA-NHS was precipitated with 10 mL of diethyl ether and centrifuged at 5,000rpm for 5 minutes at room temperature. Afterwards, the supernatant was discarded, and the polymer dissolved in 5mL of chloroform. This precipitation/dissolution washing cycle was repeated three times before the activated PLGA-NHS ester was dried under vacuum.

Synthesis of PLGA target mitochondria polymer. The PLGA-NHS polymer was dissolved in methyl sulfoxide (DMSO) (5mL), followed by the addition of *N,N*-diisopropylethylamine (DIPEA) (54μL) and the D-Arginyl Tyrosinyl Ornithinyl Phenylalanine peptide (300mg), under stirring. After 24h at room temperature, the modified polymer was precipitated by adding diethyl ether and then dried under reduced pressure.

Preparation of PLGA nanoparticles. PLGA nanoparticles were prepared by the solvent displacement technique. PLGA-NHS and PLGA-Mitochondria were dissolved in 5mL of acetone together with Coenzyme Q_{10} and poured into an aqueous solution containing poly(vinyl alcohol) at 1%, under moderate stirring for 10 minutes. The acetone was then evaporated, and the nanoparticles were concentrated under reduced pressure. Then, the target fibroblast peptide (Pentapeptide-4) was incubated with the nanoparticles under gentling stirring. After 24h at room temperature, nanoparticles were freeze-dried and redispersed in water at the desired concentration.

Rhodamine loaded PLGA nanoparticles. PLGA nanoparticles functionalized with the peptides were prepared following the procedure reported above and replacing the Coenzyme Q_{10} with 5(6)-carboxytetramethylrhodamine (Rho) (0.086g, 0.20mmol).

X-Ray photoelectron spectroscopy (XPS). The photoelectron spectroscopy experiments were performed at room temperature with a SPECS PHOIBOS 150 hemispherical analyzer (SPECS GmbH, Berlin, Germany) in a base pressure of $5x10^{-10}$ mbar using monochromatic Al Kalpha radiation (1486.74eV) as the excitation source. The water dispersion (10mg/mL) of the three samples: pure PLGA particles, particles functionalized with mitochondrial targeting peptide and particles functionalized with the two targeting peptides, were deposited on a silicon substrate and left to dry overnight. The substrates were then introduced in the ultra-high vacuum system for XPS analysis. The overview spectrums were acquired with a pass energy of 50eV and step size of 1eV, and the high-resolution spectrums were obtained with a pass energy of 20eV and step size of 0.05eV. The composition of the samples was estimated by using the area of the peaks and the proper relative sensitivity factor.

Dynamic Light Scattering (DLS) and Z-Potential Measurements. The average particle size was performed with a dynamic light scattering method using Nano ZS (Malvern Instruments, U.K.). The particle size values were obtained by averaging 10 measurements for 3 cycles at an angle of 173° at 25°C. The laser wavelength was 633nm, and measurements were performed in disposable plastic cells. The surface zeta potential was determined by electrophoretic light scattering using the same instrument and setup. The measurements were performed in a disposable capillary cell.

Transmission electron microscopy (TEM). TEM images were collected on the electron microscope Tecnai Spirit microscope (FEI, The Netherlands) equipped with a tungsten filament operated at 120kV. The sample was adsorbed onto a formvar-coated copper grid for 1 min, followed by a washing step with Milli-Q water for 1 min. Afterwards, it was negatively stained by 2% uranyl acetate.

Cell culture. Normal Human Dermal Fibroblasts (NHDF) cells were grown in human fibroblast expansion basal medium (Gibco, California, USA) supplemented with fetal bovine serum, 2% v/v, hydrocortisone (1 µg/ml), human epidermal growth factor (10ng/ml), basic

fibroblast growth factor (3ng/ml), and heparin (10µg/ml) (all acquired from Gibco, California, USA). Cells were cultured under the conditions of 5% CO_2 at 37°C.

Confocal microscopy image. A confocal laser scanning fluorescent microscope (Leica, Heidelberg, Germany) was used to observe Trojan®Q10 into the mitochondria. Briefly, NHDF cells were cultured in 6-well tissue culture plates until they reached 80% confluence. After that, PLGA nanoparticles functionalized with the targeting peptides and loaded with rhodamine were added at 0.1% concentration and left to incubate for 1h. Then Mitotracker dye was added at the concentration of 100nM incubating for 30 minutes. Successively, cells were washed and fixed with 4% *p*-formaldehyde (PFA) for 5 minutes, washed again and then incubated for 10 minutes in PBS containing 0.2% Triton® X-100, and stained with DAPI incubating for 10 minutes. Finally, cells were washed, and coverslips were mounted in slips using a fluorescence preservation medium and then observed by Leica confocal microscope with 63x objective and optical zoom.

Mitochondria membrane potential, JC-1 assay. NHDF cells were cultured overnight at a 6.000 cells/well density in a 96-well plate. After 24h, the culture medium was replaced with a fresh medium with low glucose concentration, without FBS and supplemented with Trojan®Q10 at 0.25% or free CoQ_{10} at 0.00005% concentrations. After 48h, cells were radiated with UV-A for 30 minutes (3J/cm^2, at a wavelength centered at 350nm, Luzchem Irradiator LZC-420). Non-irradiated controls were incubated at 26ºC during this time in the dark. After the irradiation period, a JC-1 working solution (2µM) was added to the wells incubating for 30 min, followed by a washing step in PBS. The fluorescence was measured at two wavelengths (530 and 590nm). JC-1 exists either as a green-fluorescent monomer at depolarized membrane potentials (~530nm) or as an orange/red-fluorescent J-aggregate at hyperpolarized membrane potentials (~590nm). The ratio of red fluorescence to green was calculated. Afterwards, images were obtained from each condition with an In-Cell Analyzer 6000 device, 20x objective, at the same wavelengths. 5-6 technical replicates per condition were used. All data were statistically analyzed using ordinary one-way ANOVA and, for direct two samples comparisons, unpaired Student's t-test. Statistical significance was set at $p < 0.05$, 95% of confidence. Graphical results were represented as Mean±SEM (Standard

Error of the Mean), analyzed statistically comparing treated vs control, and irradiated vs non-irradiated samples.

Reactive oxygen species (ROS). NHDF cells were cultured and irradiated in the same conditions reported above. After the irradiation period, MitoROS, a dye which selectively reacts with mitochondrial superoxide present in live cells, was added in all cultured wells, incubated for 1h, and fluorescence was measured in all samples (Ex/Em= 540/590nm) by Synergy H1 Hybrid Multi-mode microplate reader. The resulting emission intensity were corrected by subtracting the basal ROS production, which corresponds to the fluorescence intensity of not irradiated cells and normalizing for the irradiated control. Additionally, images were obtained with Leica inverted microscope equipped with a fluorescent lamp and camera, 20x objective. Eight technical replicates per condition were used and the data were statistically analyzed as reported for the JC-1 assay.

Collagen expression. NHDF cells were cultured overnight at a 50.000 cells/well density in a 24-wells plate, in supplemented growth media. After 24h, cells were treated with Trojan®Q10 at 0.025% for 48h. After the incubation period, specific protein levels were quantified in cell lysate. 6 replicates were used per condition. All data were statistically analyzed as reported for JC-1 assay. The formula used to analyze the raw data and to obtain the data used in the graphs was "X/M", where X is the raw value and M is the mean of the corresponding control for each replicate.

Quantification of ATP within the cells. NHDF cells were cultured in a specific growth medium for 24h in a white 96-well plate (10.000 cells/well). After the incubation period, the medium was replaced by a fresh medium with supplement (Control) or without supplement (Control low glucose) for 6h. After that, Trojan®Q10 was added for 30 minutes at concentrations of 0.025% in medium without supplement (low glucose). An untreated control was kept in a normal medium with the supplement for these 30 minutes of treatment. The amount of ATP was quantified using Luminescent ATP Detection Assay Kit measuring the luminescence by a luminometer (Synergy H1 Hybrid Multi-mode microplate reader). Six technical replicates per condition were used and the data were statistically analyzed as reported for the JC-1 assay. The data were normalized using the "Control low glucose" as reference control to detect the efficacy of the compound stimulating ATP levels.

Skin penetration study. Penetration was assessed in pig skin model according to the OECD 428 guideline. The penetration of Trojan® particles loaded with rhodamine, and free rhodamine as control, was followed by fluorescence spectroscopy. Pig-skin samples were cut into circles of 3cm diameter and mounted on the receptor compartment of a Franz diffusion cell assembly with the stratum corneum side facing upwards into the donor compartment. PBS was used as the receptor solution. An aliquot of the samples was applied onto the skin. The Franz diffusion cells were mounted on an H+P Labortechnik Variomag Telesystem (Munchen, Germany) and placed in a thermostatic bath keeping it at 32ºC. After 2h, 6h and 16h of incubation times the receptor solution was analyzed by fluorescence spectrophotometry (λ_{ex}=543nm, λ_{em}=572nm) to quantify rhodamine in the effluent. The experiment was realized in triplicates (n=3) to determine its reproducibility.

Additionally, after the incubation times, the skin sections were cut into pieces of approximately $0.5cm^2$, and the adjacent fat portion was removed. Sections were introduced into scaffolds, embedded in optimal cutting temperature compound (OCT), introduced in a container filled with isopentane and frozen in liquid nitrogen. Once the tissues are frozen, samples were stored at -80°C. Finally, a thin slice (10μm) of the samples were obtained using a cryostat. The cryosections were washed with PBS and incubated with DAPI for 20 minutes. Once stained, tissue samples were covered with fluorescence preservation medium and covered with coverslips. Samples were viewed on a Leica confocal microscope with 40x or 63x objectives.

In vivo study. A panel of 18 volunteers (40-60 years old) were submitted to a 56 days topical treatment with 1.5% Trojan®Q10 and 1% free CoQ_{10} in the facial area (twice per day, in a hemiface protocol, one treatment each side of the face). Before (Day 0) and after 56 days of treatment (Day 56), skin firmness and elasticity have been assessed in the crow's feet area through Cutometer®. Cutometer is a standard method based on the suction method where a probe creates a negative pressure, and the skin is drawn to the opening of the probe. The penetration depth is measured by non-contact optical measurement system consisting of a light source, a receiver, and two prisms, which projected light from the emitter to the receiver. The results evaluate the skin's resistance to suction (firmness) and its ability to return to its original position (elasticity).

Results.

Synthesis and characterization of Trojan®Q10 sub-micrometric particles. The delivery system, namely Trojan®Q10, was obtained starting from PLGA polymer employed as a carrier for the lipophilic antioxidant CoQ_{10} and functionalized with two different peptides (Pentapeptide-4 and D-Arginyl Tyrosinyl Ornithinyl Phenylalanine) to target specific cell lines and cellular organelles. The final particles were obtained by solved displacement technique, as disclosed in the method section.

The as obtained particles present a monodimensional distribution with a mean hydrodynamic diameter of 268.9nm and a PDI of 0.288, as determined by the DLS analysis (Figure 1A), which was also confirmed by the size distribution obtained from TEM images (Figure 1B-C). The surface potential of Trojan®Q10 particles was also measured, resulting in a negative zeta potential of 18±5.53mV ensures the colloidal stability of the nanoparticles and low cytotoxicity. [28]
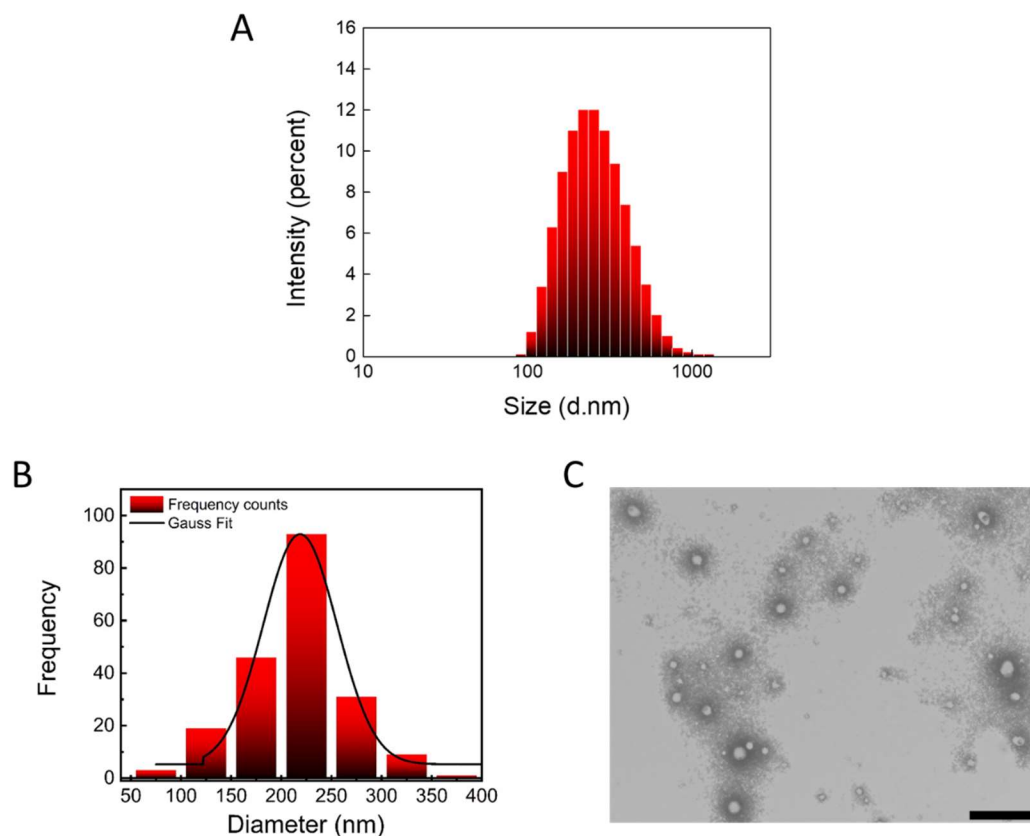

Figure 1. A) hydrodynamic diameter of the nanoparticles measured by DLS; B) size distribution of the nanoparticles obtained from TEM images analysis; C) TEM image of Trojan®Q10 particles (scale bar 1µm).

Afterwards, XPS analysis (Figure 2) was performed to verify if the peptide was exposed to the particles surface (see method section). The analysis of PLGA nanoparticles conjugated with the mito-targeting peptides (Figure 2C) shows the presence of a small peak around 400eV corresponding to the N1s core level, which is not present in the pure PLGA nanoparticles (Figure 2B). Since the peptides are the only component of the particles with N atoms, the XPS analysis confirms their presence on the surface of the final PLGA particles. Furthermore, the analysis of the PLGA particles functionalized with the two peptides (Figure 2D) showed an increase in the N concentration, from 1.1% to 1.8%, suggesting the presence of both peptide onto the nanoparticles surface.
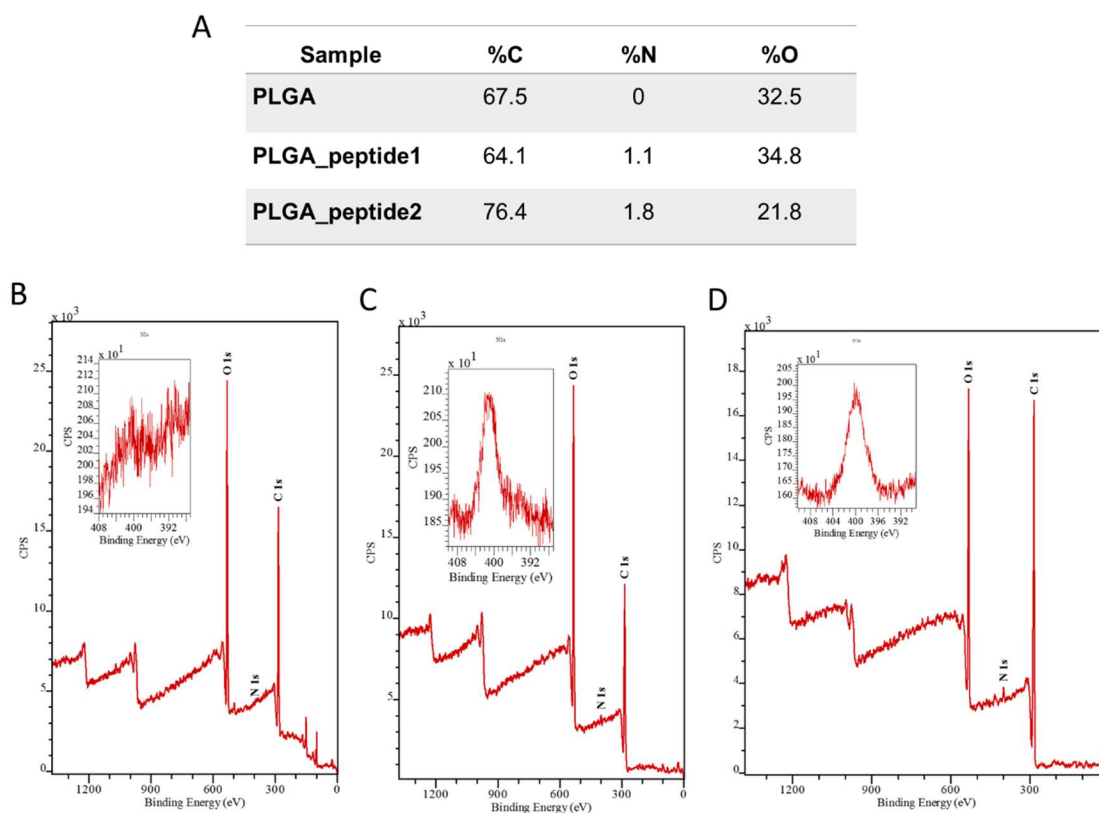

A)

Sample	%C	%N	%O
PLGA	67.5	0	32.5
PLGA_peptide1	64.1	1.1	34.8
PLGA_peptide2	76.4	1.8	21.8

Figure 2. A) Composition of the surface of the samples in the percentage of C, O and N; XPS spectra of B) PLGA particles, C) PLGA particles functionalized with mitochondrial targeting peptide and D) PLGA particles functionalized with the two peptides.

Intracellular uptake and mitochondrial localization. The efficacy of the two peptides to direct the Trojan®Q10 towards mitochondria inside Normal Human Dermal Fibroblast (NHDF) was studied by confocal microscopy (see method section). The particles internalization can be observed in Figure 3A-C, with Trojan® particles (red dots) localized

on the cell membrane. Indeed, the images show the majority of the particles at the edge of the cells, suggesting that the Trojan® particles present a high affinity for the cell membrane. At this stage, the cell penetrating peptide (Pentapeptide-4) start to interact with the fibroblast membrane inducing the particle internalization through endocytosis. Once internalized, they diffuse in the cytoplasm, as shown in Figure 3E, where an extended red fluorescence is present, indicating a high particles concentration. Thereafter, the second peptide on the particles surface, the mitochondria-penetrating peptides, start to target the mitochondria permeating its membrane. Such interaction is demonstrated by the colocalization of the particles (red dots, Figure 3E) with the mitochondria (green dots, Figure 3D) as showed in the merged confocal image reported in Figure 3F. The absence of the red signal coming from Trojan® particles outside the cell together with its overlapping with the green signal coming from the mitochondria within the cell appoint towards the efficacy of the two peptide to direct the particles to such organelles inside the fibroblasts.
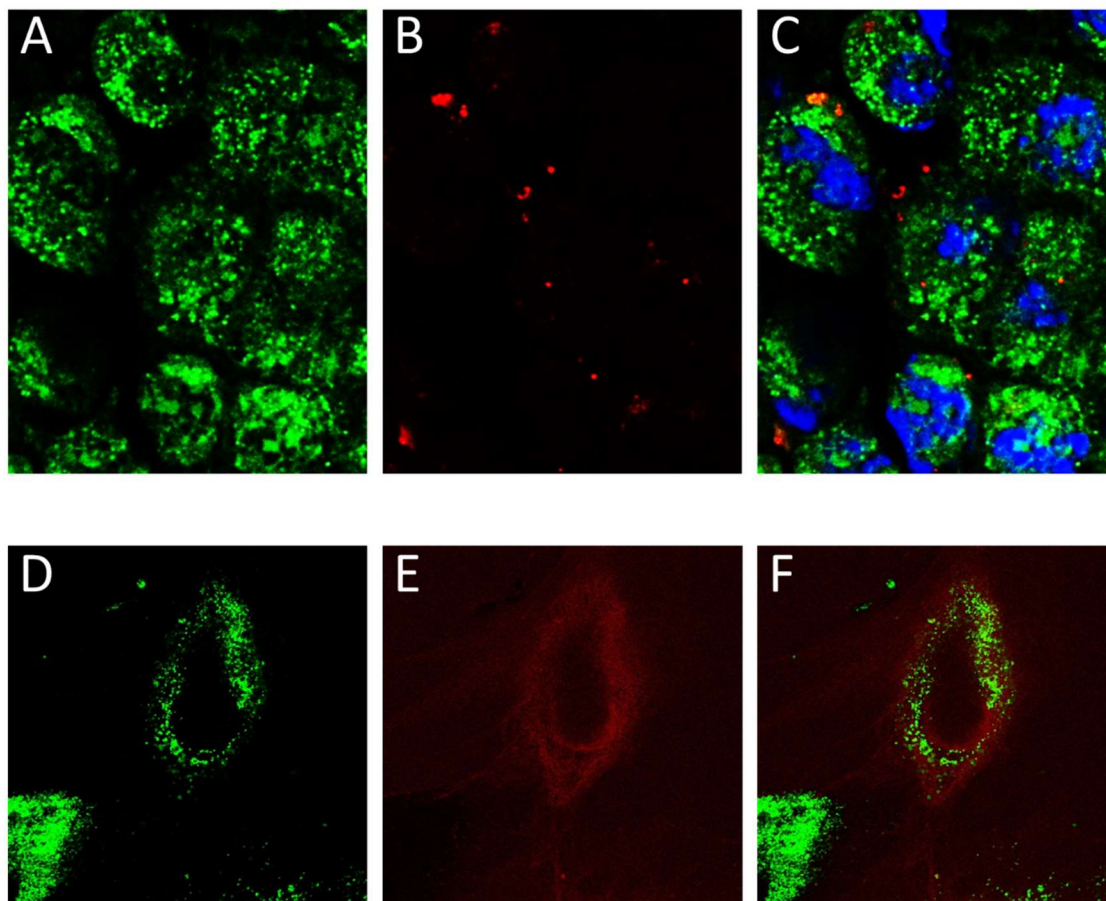
Figure 3. Confocal microscopy images of NHDF cells presenting mitochondria stained by mitotracker (green channel) (A, D), cells incubated with Trojan® particles loaded with rhodamine (red channel) (B, E), merge of the three channels showing the cells' nuclei stained with DAPI (blu channel), the cells mitochondria, and the nanoparticles (C). Merge of the two confocal channels showing the cell mitochondria, and the internalized nanoparticles colocalized with the mitochondria (F).

Protective action of Trojan®Q10 on mitochondria against oxidative stress. Short- (280–320nm) and long-waved (320–400nm) UV, also named UVA and UVB, respectively, are known to stimulate the intracellular synthesis of ROS, which have been implicated in skin ageing.[29] UVA irradiation was used to induce oxidative stress in the mitochondria of NHDF so to evaluate the activity of Trojan®Q10 on preventing the damage of the mitochondria from the as produced ROS.

The electrical potential of the mitochondria membrane controls, among others, ATP synthesis and ROS generation, being an important physiological parameter employed to monitor the health states of cells.[30] Indeed, hyperpolarization and depolarization of mitochondrial membrane are linked to mitochondrial damage leading to cellular apoptosis.[31-

[32] Mitochondrial membrane potential can be measured using JC-1 dye, which emits green fluorescence (~530nm) in depolarized mitochondria, or red fluorescence (~590nm) in hyperpolarized mitochondria with membrane potentials more negative than −140mV.

Thus, the JC-1 assay was employed to monitor the MMP after cells exposure to UVA, in the presence of Trojan®Q10 (0.25%), free Coenzyme Q_{10} (0.00005%, the equivalent concentration of Q_{10} into the particle), and in their absence. When the cells are irradiated with UVA, the emission of JC-1 dye at 590nm increases by 67.4±8.3%, compared to the not irradiated cells, indicating the hyperpolarization of the mitochondrial membrane (Figure 4A). The NDHF cells treated with Trojan®Q10 showed a reduced hyperpolarization, by 32.2±8.2% compared to the control, suggesting the protective action of the particles upon the mitochondria. Furthermore, the cells treated with free CoQ_{10} showed similar hyperpolarization of the irradiated control, pointing out the efficacy of the encapsulation in boosting the ubiquinone activity. The same tendency was observed, measuring the ratio between red (polarized state) and green (depolarized state) of the dye, which indicates the depolarization of mitochondria membranes (Figure 4B). The results showed that UVA irradiation of untreated NDHF significantly increased the ratio red/green by 47.8±6.4%, whereas the treatment with Trojan®Q10 significantly decreased it by 30.2±7.1%. Also, in this case, no significant effect was observed after treatment with free CoQ_{10}, compared to the irradiated control.

These results were confirmed by observing the fluorescence microscopy images reported in Figure 4C-D. The UVA-induced increase of hyperpolarized and total membrane potential is observed with higher red (590nm) fluorescence (Figure 4C) and yellow (ratio 590/530nm) fluorescence (Figure 4D). When the Trojan®Q10 treated cells are compared with the irradiated control, it is possible to observe a decrease in the red and yellow emission, confirming the protective action exerted by the nanoparticles.
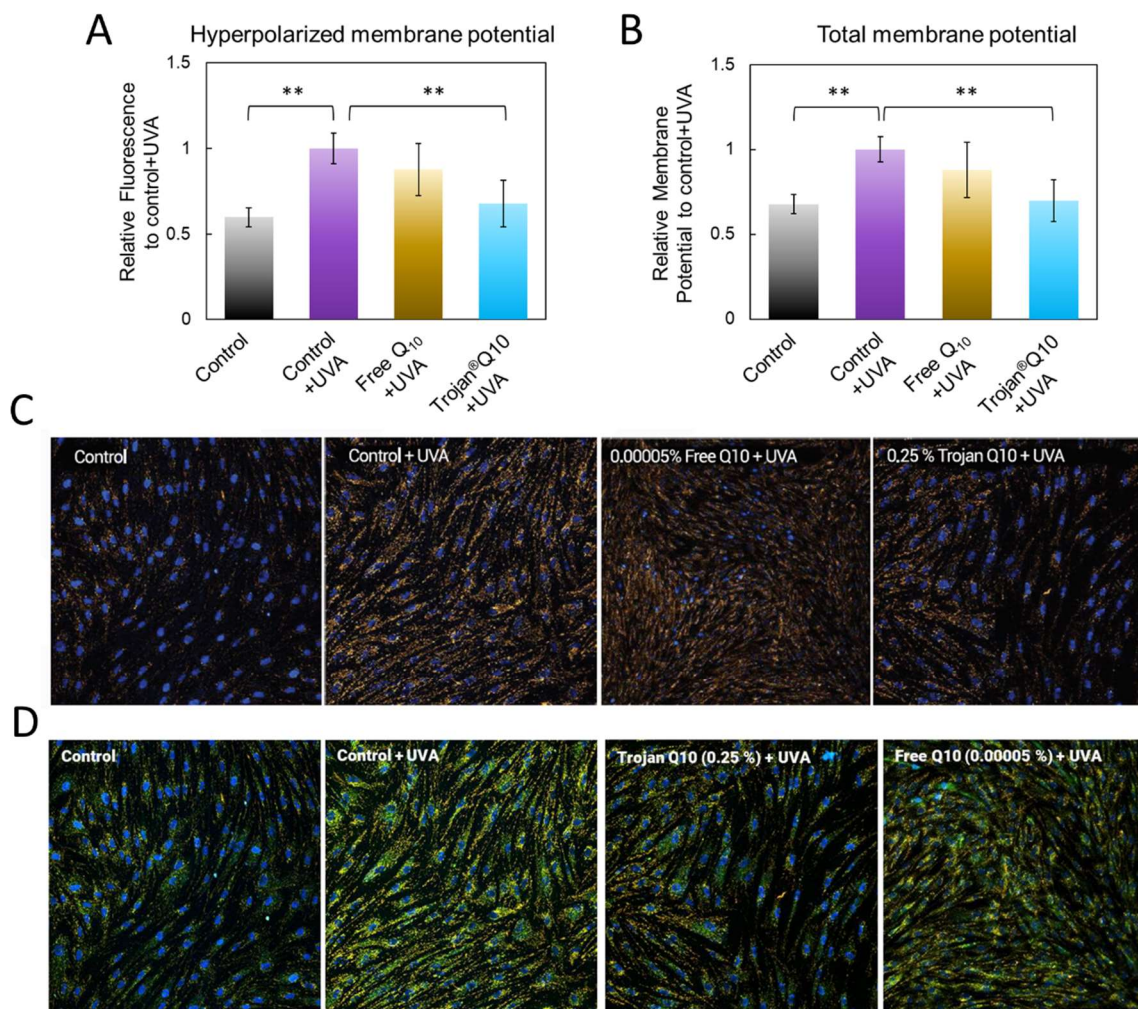
Figure 4. JC-1 assay performed after the exposure of the cells to UVA. A) Hyperpolarized and B) total mitochondria membrane potential obtained measuring the fluorescence of JC-1 dye at 590nm and the ratio 590/530nm, respectively. C) Fluorescence microscope images of NHDF cells (control), cells after exposure to UV-A (Control+UVA), and cells incubated with free CoQ$_{10}$ or Trojan®Q10 particles after irradiation with UV-A. The red fluorescence comes from JC-1 dye aggregates. D) Fluorescence microscope images of NHDF cells (control), cells after exposure to UV-A (Control+UVA), and cells incubated with free CoQ$_{10}$ or Trojan®Q10 particles after irradiation with UV-A. The green/yellow fluorescence comes from JC-1 dye monomer. The nuclei are stained with DAPI (blu).

The activity of Trojan®Q10 upon the reduction of oxidative stress in mitochondria was also assessed measuring the level of ROS production induced after UVA irradiation of the cells, (see method section). In Figure 5A is reported the emission intensity of the irradiated control and the cells treated with the Trojan®Q10 at two different concentrations (0.25% and 0.025%). The results showed a significant reduction of mitochondrial ROS production and accumulation in cells treated with Trojan®Q10 of about 10.5±3.2% and 19.3±2.9%, for the 0.025% and 0.25% concentrations, respectively. The reduction in the MitoROS fluorescence

can also be appreciated from the fluorescence microscope images of the cells reported in Figure 5B.
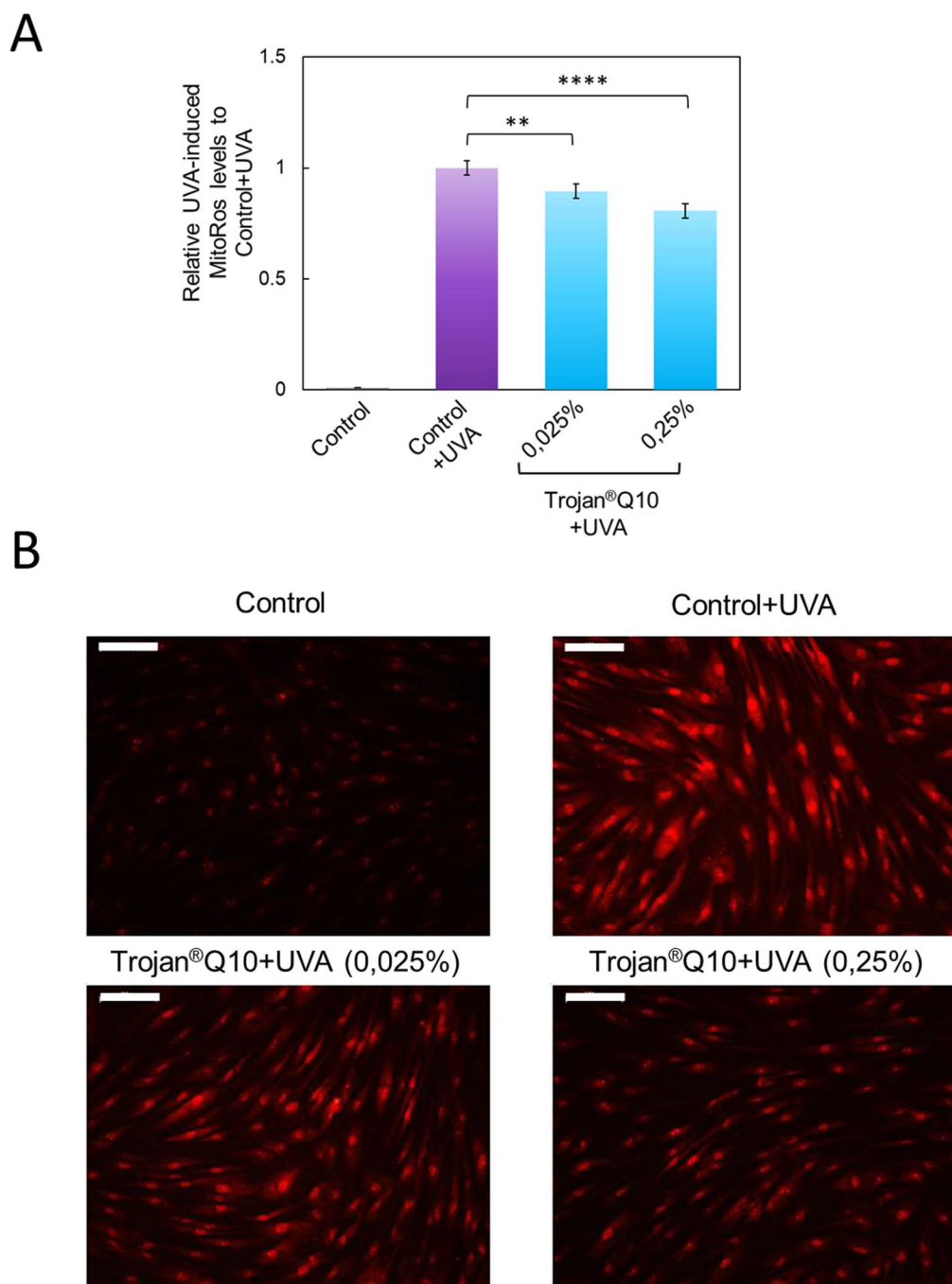

Figure 5. A) ROS level of NHDF cells irradiated by UV-A determined measuring the emission intensity of ROS sensitive dye mitoROS. B) Fluorescence microscope images of the NHDF cells irradiated with UV-A and stained with mitoROS of the not treated cells (control), cells exposed to UV-A (control+UVA), and cells treated with Trojan®Q10 particles at the two concentrations: 0.25% and 0.025%. (Scale bar 100µm).

The studies presented above have demonstrated the protective action of Trojan®Q10 on mitochondria against oxidative stress induced by external agents. However, the excessive production of ROS species by mitochondria can be the consequence of different conditions, as in the mitochondria metabolic dysfunctions. For example, glucose starvation can lead to decreased ATP production and increased ROS generation. Thus, the reduction of oxidative stress on mitochondria by Trojan®Q10 was also investigated in NHDF cells exposed to a starvation period and successively treated with the particles (see method section). The results reported in Figure 6 showed a decrease of the ATP levels in the untreated cells undergoing glucose-starvation compared to the control in normal conditions. When the Trojan®Q10 is added, ATP level are completely recovered to similar value of the control cells in normal conditions.
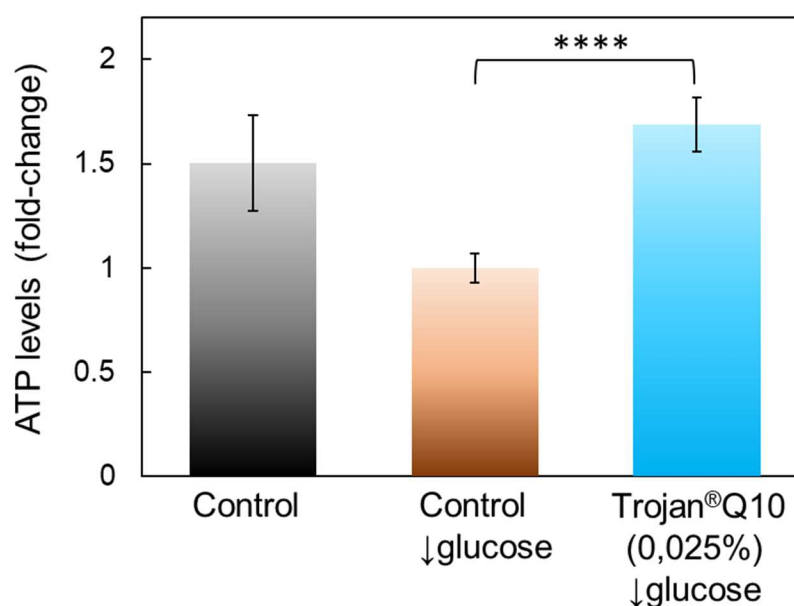

Figure 6. Amount of ATP level determined by ATP Detection Assay Kit of NHDF cells untreated (control), cells exposed to a starvation period (control glucose) and cells exposed to a starvation period incubated with Trojan®Q10 at 0.25%.

This analysis further confirms the protective action of Trojan®Q10 on mitochondria upon oxidative stress, which in this case is reflected as a stimulating effect on cellular metabolism of fibroblasts.

A further consequence of the mitochondria oxidative stress usually involves the mtDNA deletion, which are implicated in degenerative diseases and premature ageing.[33] In literature

has been reported that deletions in mtDNA in human dermal fibroblasts could lead to a sensible reduction of collagen fibers in the surrounding extracellular matrix.[34]

Finally, to confirm the protective action of Trojan®Q10 on mitochondria from oxidative stress, we investigate the changes in the collagen expression in NHDF cells treated with the particles compared to untreated cells (see method section). The results reported in Figure 7 showed an increase of protein production, specifically Trojan®Q10 promoted collagen type IV and type VII synthesis by 39% and 27% respectively.
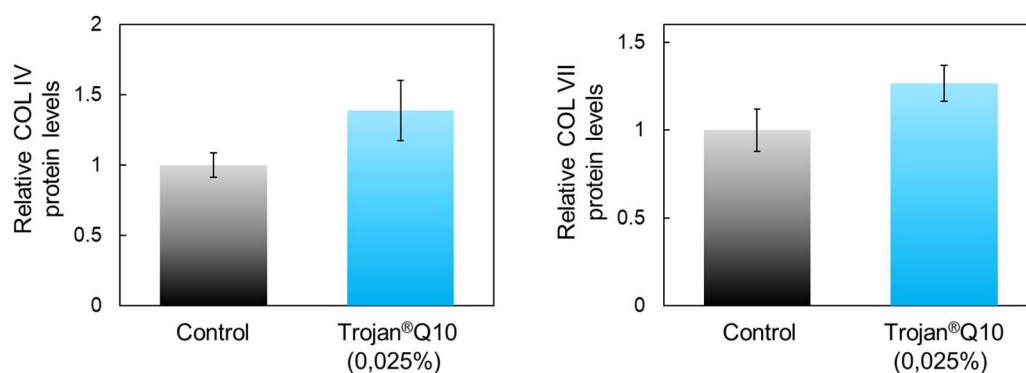

Figure 7. Stimulation of Collagen IV and VII production in NHDF cells after treatment with 0.025% Trojan®Q10.

Skin penetration of Trojan®Q10. The ability of Trojan®Q10 to penetrate through the different skin layers was investigated by performing the penetration study using pig-skin (see method section). The penetration profile reported in Figure 8A shows a fast penetration of Trojan® particles compared to the control, with 65% of the particles penetrated after 2h and 90% after 6h. Moreover, 100% of Trojan® pass through the skin after 20h, against only 35% of the free rhodamine, pointing out the high efficiency of Trojan® particles in delivering the active across the skin layers.

The localization of Trojan® particles at different skin layer was also determined by confocal microscopy. The images of pig-skin sections at different times reported in Figure 8B confirms the fast penetration of Trojan® particles, showing most of the particles crossing the epidermis and reaching the deep layer of the dermis already after 2h.
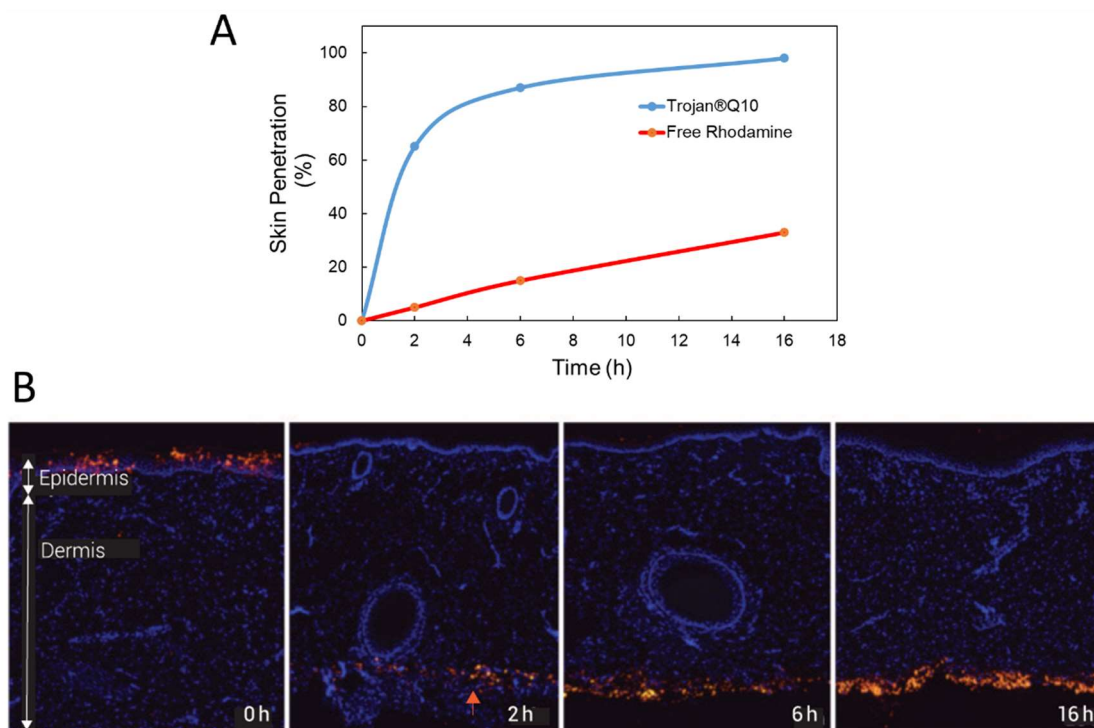
Figure 6. A) Skin penetration profile of Trojan® particles loaded with rhodamine and free rhodamine as control determined by fluorescence spectroscopy. B) Confocal microscope images of the pig-skin section with Trojan® particles (red spot) at different times showing the penetration of the particles across the skin layers (blue spots represents cell nuclei).

In vivo study: firmness and elasticity. The clinical efficacy of Trojan®Q10 as anti-aging has been evaluated in terms of firmness and elasticity assessing the crow's feet area in a panel of 18 volunteer before (Day 0) and after 56 days of treatment (Day 56), using free CoQ_{10} as a control (see method section).

The in vivo topical treatment in the volunteers during 56 days with Trojan®Q10 displays antiaging effects, through significant increase of skin firmness by 10% and elasticity by 14% (Figure 9A-B). The Trojan®Q10 exhibited a two times higher efficacy for the skin elasticity when compared with free CoQ_{10} treatment. Worth to mentioning that the coenzyme CoQ_{10} concentration within the Trojan®Q10 capsules is 3000 times lower than the dose of CoQ_{10} used as control in the clinical study.
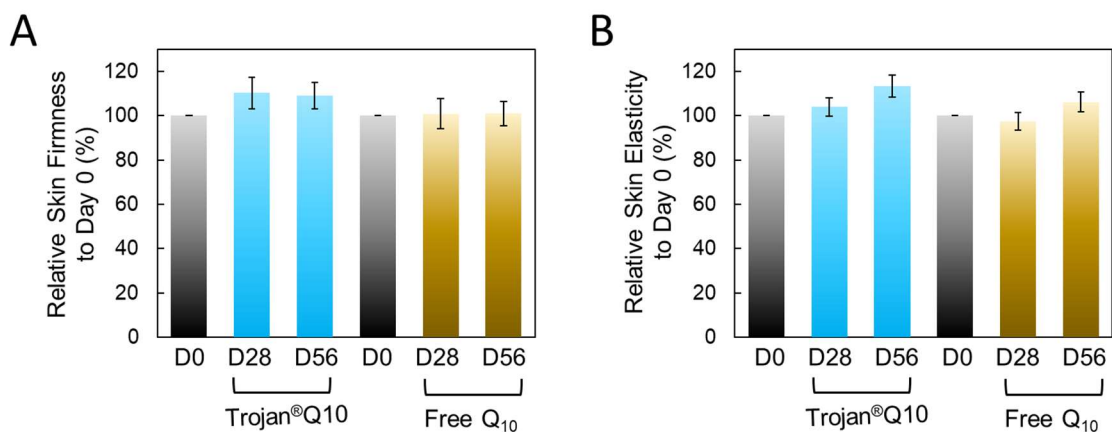
Figure 7. In vivo assessment of anti-aging capacity of 1.5% Trojan®Q10 vs 1% free CoQ$_{10}$ treatment. A) Firmness and B) elasticity data collected after 28 and 56 days.

The 2D images of the selected area and its topography of a representative volunteer are reported in Figure 10. From the analysis of the images a significant reduction of fine lines can be appreciated in the case of Trojan®Q10 application and, in particular, a 25% reduction of lines area and length can be observed.
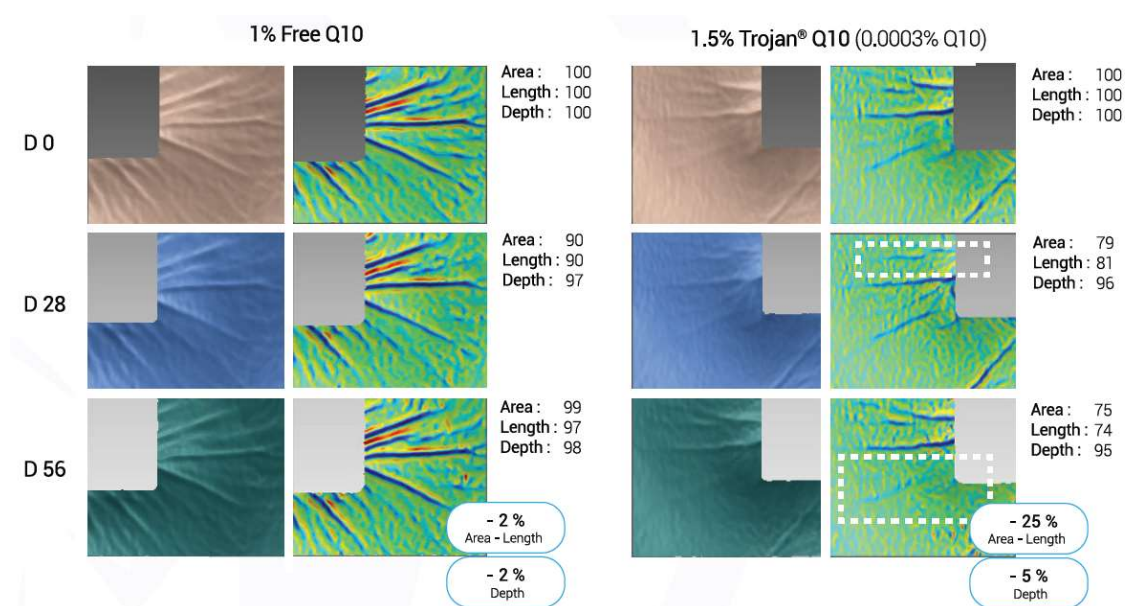

Figure 8. The 2D images of the selected area and its topography of a representative volunteer showing the difference in efficacy between the treatment with the control (free CoQ$_{10}$) and the Trojan®Q10.

Discussion.

In this study we have shown that Trojan®Q10 is able to specifically target mitochondria within fibroblast cells releasing Coenzyme Q$_{10}$ and effectively protect the organelle from

oxidative stress, in turns increasing the collagen IV and VII production and stimulating the cellular metabolism restoring the ATP levels within the cell.

So far, the physicochemical characterization of Trojan®Q10 presented here confirms the formation of monodispersed PLGA sub-micrometric particles and their functionalization with the two peptides, targeting fibroblasts and mitochondria.

Thereafter, the in vitro assays clearly attest the targeting properties and the antioxidant activity of Trojan®Q10. The confocal microscopy analysis of NHDF incubated with labelled Trojan® particles display their ability to specifically address mitochondria within fibroblast. Remarkably, the JC-1 assays and the fluorescence microscopy study distinctly demonstrate the antioxidant activity of Trojan®Q10 through a protective and energizing action on the mitochondria manifested by the restoring of mitochondrial membrane potential and ATP levels together with the reduction in ROS level after exposing the cell to UVA. Such protective action of Trojan®Q10, was also reflected on increasing production of collagen IV and VII, which in turns gives a more firmness skin.

The in vitro results prove the efficacy of Trojan®Q10 to target and protect mitochondria within fibroblast, but as a delivery system it may be able to cross the different skin layers to reach such targets. Moreover, the skin, as a protective layer, is exposed to various damaging agents,[35-37] thus being a major target of oxidative stress. Therefore, penetration study was performed showing a fast penetration of the Trojan®Q10, with 90% of the particles crossing the epidermis and reaching the deep layer in 6 hours.

Finally, the results obtained by in vitro assay was proved in clinical study, where topical treatment with Trojan®Q10 displays antiaging effects, through significant increase of skin firmness and elasticity. Thus, this study demonstrates the ability of Trojan® particles to protect while effectively delivering the Coenzyme Q_{10} across the skin toward fibroblast mitochondria, where the protective and energizing action of CoQ_{10} take place employing lower doses than formulation with not encapsulated CoQ_{10}.

Conclusion.

In summary, we have developed a fibroblast, and mitochondrial targeting Coenzyme Q_{10} loaded PLGA particles delivery system (namely Trojan®Q10), which offers a significant

benefit because it allows the specific delivery of active molecule to subcellular targets without the need for chemical modification of the bioactive agents, enhancing its stability and penetration. Most importantly, we have shown that such mitochondrial specific CoQ_{10} loaded carriers can significantly strengthen the protection of the mitochondria from oxidative stress-induced either by external agents or metabolic dysfunctions, and it effectively increase collagen synthesis. Moreover, we have also demonstrated the ability of Trojan®Q10 particles to cross the skin layers preserving their integrity until they reach the targeted cells. Finally, the in vivo study confirmed the efficacy of Trojan®Q10 treatment, which leads to a rejuvenated skin appearance, with increased elasticity and firmness.

Conflict of Interest Statement. NONE.

References.

1. Moreira PI, Zhu X, Wang X, et al (2010) Mitochondria: A Therapeutic Target in Neurodegeneration. Biochim Biophys Acta 1802:212−220.

2. Yamada Y, Harashima H (2008) Mitochondrial drug delivery systems for macromolecule and their therapeutic application to mitochondrial diseases. Adv Drug Delivery Rev 60:1439−1462.

3. Oyewole AO, Birch-Machin MA (2015) Mitochondria-targeted antioxidants. FASEB J 29:4766-71.

4. Soeur J, Eilstein J, L´ereaux G, et al (2015) Skinresistance to oxidative stress induced by resveratrol: fromNrf2 activation to GSH biosynthesis. Free Radic Biol Med 78:213–223.

5. Gioscia-Ryan RA, LaRocca TJ, Sindler AL, et al (2014) Mitochondria-targeted antioxidant (MitoQ) ameliorates age-related arterial endothelial dysfunction in mice. J Physiol 592:2549–2561.

6. López-Otín C, Galluzzi L, Freije JMP, et al (2016) Metabolic Control of Longevity. Cell 166:802-821.

7. Ziada Adam S, Smith Marie-Soleil R, Côté Hélène CF (2020) Updating the Free Radical Theory of Aging. Front Cell Dev Biol 8: 575645.

8. Korshunov SS, Skulachev VP, and Starkov AA (1997) High protonic potential actuates a mechanism of production of reactive oxygen species in mitochondria. FEBS Lett 416:15–18.

9. Hansford RG, Hogue BA, and Mildaziene V (1997) Dependence of H_2O_2 formation by rat heart mitochondria on substrate availability and donor age. J Bioenerg Biomembr 29:89–95.

10. Votyakova TV, Reynolds IJ (2001) DeltaPsi(m)-Dependent and -independent production of reactive oxygen species by rat brain mitochondria. J Neurochem 79:266–277.

11. Miwa S, Brand MD (2003) Mitochondrial matrix reactive oxygen species production is very sensitive to mild uncoupling. Biochem Soc Trans 31:1300–1301.

12. Turunen M, Olsson J, Dallner G (2004) Metabolism and function of coenzyme Q. Biochim Biophys Acta. 1660:171-99.

13. Danhier F, Ansorena E, Silva JM, et al (2012) PLGA-based nanoparticles: An overview of biomedical applications. J Control Release 161:505-522.

14. Santra S, Yang H, Stanley JT, et al (2005) Rapid and effective labeling of brain tissue using TAT-conjugated CdS:Mn/ZnS quantum dots. Chem Commun 25:3144–3146.

15. Delehanty JB, Medintz IL, Pons T, et al (2006) Enhancing the Stability and Biological Functionalities of Quantum Dots via Compact Multifunctional Ligands. Bioconjugate Chem 17:920–927.

16. Rothbard JB, Garlington S, Lin Q, et al Conjugation of arginine oligomers to cyclosporin A facilitates topical delivery and inhibition of inflammation. Nat Med 6:1253-1257.

17. Nasrollahi SA, Taghibiglou C, Azizi E, and Farboud ES (2012) Cell-penetrating Peptides as a Novel Transdermal Drug Delivery System. Chem Biol Drug Des 80: 639-646.

18. Gupta B, Levchenko TS, Torchilin VP (2005) Intracellular delivery of large molecules and small particles by cell-penetrating proteins and peptides. Adv Drug Deliv Rev 57:637-651.

19. Jones A, Sayers E (2012) Cell entry of cell penetrating peptides: tales wagging dogs. J Control Release 161:582–591.

20. Joliot A, Prochiantz A Transduction peptides: from technology to physiology. Nat Cell Biol 6:189-196.

21. Snyder EL, Dowdy SF (2004) Cell-penetrating peptides in drug delivery. Pharm Res 21:389-393.

22. Futaki S, Nakase I, Tadokoro A, et al (2007) Arginine-rich peptides and their internalization mechanisms. Biochem Soc Trans 35:784-787.

23. Henriques ST, Costa J, Castanho MA (2005) Re-evaluating the role of strongly charged sequences in amphipathic cell-penetrating peptides: a fluorescence study using Pep-1. FEBS Lett 579:4498-4502.

24. Terrone D, Sang SL, Roudaia L, Silvius JR (2003) Penetratin and ated cell-penetrating cationic peptides can translocate across lipid bilayers in the presence of a transbilayer potential. Biochemistry 42:13787-13799.

25. Zhang L, Wang D, Yang K, et al (2018) Mitochondria-Targeted Artificial "Nano-RBCs" for Amplified Synergistic Cancer Phototherapy by a Single NIR Irradiation. Adv Sci 5:1800049.

26. Luo S, Tan X, Fang S, et al (2016) Mitochondria-targeted small-molecule fluorophores for dual modal cancer phototherapy. Adv Funct Mater 26:2826–2835.

27. Szeto HH (2006) Mitochondria-targeted peptide antioxidants: novel neuroprotective agents. AAPS J. 8:E521–E531.

28. Shao XR, Wei XQ, Song X, et al (2015) Independent effect of polymeric nanoparticle zeta potential/surface charge, on their cytotoxicity and affinity to cells. Cell Prolif 48:465–474.

29. Adelman R, Saul RL, Ames BN (1988) Oxidative damage to DNA: relation to species metabolic rate and life span. Proc Natl Acad Sci USA 85:2706–2708.

30. Li J, Kwon N, Jeong Y, et al (2018). Aggregation-Induced Fluorescence Probe for Monitoring Membrane Potential Changes in Mitochondria. ACS Appl Mater Interfaces 10:12150-12154.

31. Jin F, Liu D, Yu H, et al (2019) Sialic Acid-Functionalized PEG-PLGA Microspheres Loading Mitochondrial-Targeting-Modified Curcumin for Acute Lung Injury

Therapy. Mol Pharm 16:71–85.

32. Banki K, Hutter E, Gonchoroff N, Perl A (1999) Elevation of mitochondrial transmembrane potential and reactive oxygen intermediate levels are early events and occur independently from activation of caspases in Fas signaling. J Immunol 162:1466-1479.

33. Loeb LA, Wallace DC, Martin GM (2005) The mitochondrial theory of aging and its relationship to reactive oxygen species damage and somatic mtDNA mutations. Proc Natl Acad Sci USA 102:18769-18770.

34. Schroeder P, Gremmel T, Berneburg M, Krutmann J (2008) Partial depletion of mitochondrial DNA from human skin fibroblasts induces a gene expression profile reminiscent of photoaged skin. J Invest Dermatol 128:2297-2303.

35. Schalbreuter KU, Wood JM (1989) Free radical reduction in the human epidermis Free Rad Biol Med 6:519-532.

36. Kohen R, Fanberstein D, Tirosh O (1997) Reducing equivalents in the aging process Arch Gerontol Geriatr 24:103123.

37. Rieger MM, Pains M (1993) Oxidative reactions in and on the skin: mechanism and prevention. Cosmetic Toiletries 108:43–56.